Acta Crystallographica Section F
Structural Biology and Crystallization Communications
ISSN 1744-3091

The structure of substrate-free 1,5-anhydro-D-fructose reductase from *Sinorhizobium meliloti* 1021 reveals an open enzyme conformation

Mario Schu,[a]‡ Annette Faust,[a]‡ Beata Stosik,[b] Gert-Wieland Kohring,[b] Friedrich Giffhorn[b] and Axel J. Scheidig[a]*

[a]Institute of Zoology – Structural Biology, Christian-Albrechts University Kiel, Am Botanischen Garten 1-9, 24118 Kiel, Germany, and [b]Lehrstuhl für Angewandte Mikrobiologie, Universität des Saarlandes, 66041 Saarbrücken, Germany

‡ These authors contributed equally to this work.

Correspondence e-mail: axel.scheidig@strubio.uni-kiel.de

Received 26 May 2013
Accepted 15 July 2013

PDB Reference: 1,5-anhydro-D-fructose reductase, 4koa

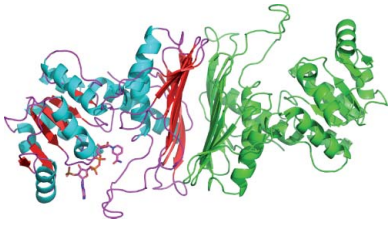

1,5-Anhydro-D-fructose (1,5-AF) is an interesting building block for enantioselective and stereoselective organic synthesis. Enzymes acting on this compound are potential targets for structure-based protein/enzyme design to extend the repertoire of catalytic modifications of this and related building blocks. Recombinant 1,5-anhydro-D-fructose reductase (AFR) from *Sinorhizobium meliloti* 1021 was produced in *Escherichia coli*, purified using a fused 6×His affinity tag and crystallized in complex with the cofactor NADP(H) using the hanging-drop technique. Its structure was determined to 1.93 Å resolution using molecular replacement. The structure displays an empty substrate-binding site and can be interpreted as an open conformation reflecting the enzyme state shortly after the release of product, presumably with bound oxidized cofactor $NADP^+$. Docking simulations indicated that amino-acid residues Lys94, His151, Trp162, Arg163, Asp176 and His180 are involved in substrate binding, catalysis or product release. The side chain of Lys94 seems to have the ability to function as a molecular switch. The crystal structure helps to characterize the interface relevant for dimer formation as observed in solution. The crystal structure is compared with the structure of the homologue from *S. morelense*, which was solved in a closed conformation and for which dimer formation in solution could not be verified but seems to be likely based on the presented studies of *S. meliloti* AFR.

1. Introduction

The sugar 1,5-anhydro-D-fructose (1,5-anhydro-D-*arabino*-hex-2-ulose; 1,5-AF) is the central intermediate of the so-called anhydrofructose pathway, an alternative starch- and glycogen-degrading pathway in bacteria, fungi, plants and mammals (Yu, 2008; Yu & Fiskesund, 2006). 1,5-AF is produced by α-(1,4)-glucan lyase (EC 4.2.2.13), which catalyses the release of 1,5-AF from the nonreducing end of α-(1,4)-glucans (Lee *et al.*, 2003; Yu *et al.*, 1993) or *via* the microsomal glycosidase II as a side product during the catabolic degradation of maltose (Andersen *et al.*, 2002*b*; Hirano *et al.*, 2000). In *Escherichia coli*, higher plants and mammalian tissues, the half-life of 1,5-AF is short as it is instantly reduced to 1,5-anhydro-D-glucitol (1,5-AG) by a specific NADPH-dependent anhydrofructose reductase (Sakuma *et al.*, 1998). Since only a small fraction of α-(1,4)-glucans are degraded *via* the anhydrofructose pathway (Yu & Pedersén, 1993; Yu *et al.*, 1993, 2004), it was assumed that 1,5-AF or 1,5-AG could play regulatory roles in glycogen metabolism (Kametani *et al.*, 1996; Konishi *et al.*, 2000). In *E. coli* 1,5-AG promotes glycogenolysis (Shiga *et al.*, 1999) and in mammals 1,5-AF or 1,5-AG stimulates insulin secretion (Yamanouchi *et al.*, 2003). Although little is known about the physiological importance of 1,5-AF and 1,5-AG in human glucose homeostasis, differences in 1,5-AG serum concentrations between healthy and diabetic individuals have been observed, rendering 1,5-AG an established marker in diabetic control (Dworacka & Winiarska, 2005; Kim *et al.*, 2011). Clinical trials have been proposed to use 1,5-AF and its derivatives against sugar metabolism disorder-related diseases (Ahrén *et al.*, 2000; Ahrén & Yu, 2002). For a recent review of the relevance of 1,5-AF to medical applications, see Fiskesund *et al.* (2010). 1,5-AF has considerable relevance to the field of white biotechnology since it can serve as a chiral building block for organic synthesis (Andersen *et al.*, 2002*b*; Lundt & Yu, 2010). In this

respect, the identification and characterization of enzymes utilizing 1,5-AF as a substrate is of specific interest.

By microbial screening using 1,5-AF as the sole carbon source, a novel 1,5-AF reductase (AFR; EC 1.1.1.292) was found in *Sinorhizobium morelense* S-30.7.5 (Kühn *et al.*, 2006) which catalyses the stereoselective and quantitative reduction of 1,5-AF to 1,5-anhydro-D-mannitol (1,5-AM; Fig. 1). In contrast to the regulatory role of AFR in mammals, this bacterial AFR is a metabolic enzyme.

The AFR from *S. morelense* was assigned to the GFO/IDH/MocA family and its general occurrence among the Rhizobiaceae has been demonstrated (Kühn *et al.*, 2006). This family is composed of enzymes that utilize NADP or NAD as a redox cofactor. Glucose–fructose oxidoreductase (GFOR; Zachariou & Scopes, 1986; Kingston *et al.*, 1996), *myo*-inositol dehydrogenase (IDH) and the dehydrogenase MocA of rhizopine catabolism are representative members of this family. 1,5-AF can be synthesized biocatalytically from starch by 1,4-glucanlyase and pullulanase and is a cheap resource for various chemical and biocatalytical transformations, *e.g.* as a building block for enantioselective and stereoselective organic synthesis (Andersen *et al.*, 2002*b*; Lichtenthaler *et al.*, 1980; Lundt & Yu, 2010). 1,5-AF can also be used for a variety of applications in the food and pharmaceutical industries, *e.g.* as a low-calorie sweetener (Andersen *et al.*, 2002*a*) and antioxidant (Fujisue *et al.*, 2003; Susumu *et al.*, 2003) or as a humectant (Susumu *et al.*, 2002). The crystal structure of AFR from *S. morelense* has recently been determined and published (Dambe *et al.*, 2006). In contrast to *S. morelense*, the complete genome of *S. meliloti* 1021 is known (Capela *et al.*, 2001), which provides access to putative enzymes in 1,5-AF metabolism. Therefore, this organism is currently used as a model organism for further characterization of the 1,5-anhydro-D-fructose pathway in Rhizobiaceae. The *afr* gene from *S. meliloti* has 1002 base pairs and the derived polypeptide showed 86% identity to the AFR from *S. morelense*. The enzyme was cloned and heterologously expressed in *E. coli* for further biochemical characterization and comparison with the *S. morelense* reductase. To provide a solid basis for rational protein design, we prepared crystals for determination of its three-dimensional structure. Here, we present the crystal structure of AFR from *S. meliloti* and describe the observed differences from AFR from *S. morelense* and GFOR.

2. Materials and methods

Recombinant AFR from *S. meliloti* 1021 was produced in *E. coli* BL21(DE3)Gold cells fused with an N-terminal 6×His affinity tag including a factor Xa protease cleavage site using pET-24a(+) as the expression vector with a stop codon prior to its C-terminal 6×His affinity tag. After purification by Ni–NTA affinity chromatography and cleavage of the N-terminal 6×His affinity tag by 24 h incubation with the protease factor Xa, the protein was purified to homogeneity by Q Sepharose anion-exchange chromatography.

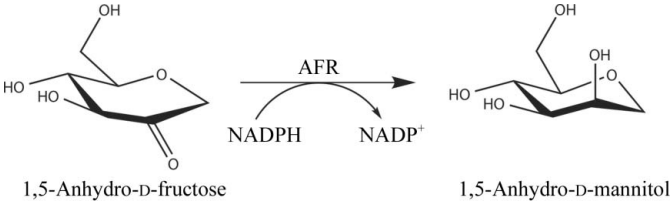

Figure 1
The reaction catalyzed by 1,5-anhydro-D-fructose reductase (AFR; EC 1.1.1.292) from *S. meliloti*. 1,5-Anhydro-D-fructose (1,5-AF) is a cyclic ether and not a hemiacetal since it lacks the hydroxyl group at the C1 position. It is stereoselectively reduced to 1,5-anhydro-D-mannitol (1,5-AM) by AFR. For the enzymatic reduction the enzyme utilizes the cofactor NADPH. This is the first step in the 1,5-AF pathway as first shown for *S. morelense* (Kühn *et al.*, 2006).

Table 1
Diffraction data-collection and refinement statistics.

Values in parentheses are for the highest resolution shell.

Wavelength (Å)	1.5418
Temperature (K)	100
Space group	$C222_1$
Unit-cell parameters (Å)	a = 68.9, b = 89.7, c = 94.5
Resolution (Å)	19.5–1.93 (1.98–1.93)
Unique reflections	22202 (1487)
Completeness (%)	99.2 (91.5)
Multiplicity	14.3 (12.6)
$\langle I/\sigma(I)\rangle$	26.9 (4.7)
Wilson B factor (Å^2)	24.6
$R_{\rm meas}$† (%)	10.4 (63.9)
$R_{\rm work}$‡ (%)	15.4 (18.6)
$R_{\rm free}$§ (%)	20.7 (24.7)
No. of non-H atoms	
Protein	2449
Solvent	291
Cofactor	48
Average B factor (Å^2)	
Protein	22.3
Waters	28.5
Cofactor	69.5
Cruickshank DPI¶ (Å)	0.141
Ramachandran plot††	
Most favoured (%)	90.0
Additionally and generously allowed (%)	9.6
Outliers (%)	0.4
R.m.s.d. from ideal values‡‡	
Bond lengths (Å)	0.02
Bond angles (°)	2.05
PDB code	4koa

† $R_{\rm meas} = 100 \times \sum_{hkl}\{N(hkl)/[N(hkl)-1]\}^{1/2}\sum_i |I_i(hkl) - \langle I(hkl)\rangle|/\sum_{hkl}\sum_i I_i(hkl)$, where $I_i(hkl)$ is the intensity of the ith individual measurement of the reflection with Miller indices hkl and $\langle I(hkl)\rangle$ is the mean intensity of all measurements of $I(hkl)$ calculated for $I \geq 3\sigma(I)$; $N(hkl)$ is the redundancy or multiplicity of the observed reflection (Diederichs & Karplus, 1997; Weiss, 2001). ‡ $R_{\rm cryst} = 100 \times \sum_{hkl}||F_{\rm obs}| - |F_{\rm calc}||/\sum_{hkl}|F_{\rm obs}|$, where $F_{\rm obs}$ and $F_{\rm calc}$ are the observed and calculated structure-factor amplitudes, respectively. § $R_{\rm free}$ is equivalent to $R_{\rm cryst}$ but is calculated from reflections (5%) that were omitted from the refinement process (Brünger, 1992; Tickle *et al.*, 2000). ¶ Diffraction-component precision index (Cruickshank, 1999) calculated using the program *SFCHECK* (Vaguine *et al.*, 1999). †† Calculated using the program *PROCHECK* (Laskowski *et al.*, 1993). ‡‡ From standard geometry using the Engh and Huber library (Engh & Huber, 1991).

In order to obtain reasonably sized single crystals of AFR, microseeding and macroseeding steps were performed. In the end, small crystals of AFR grew in a solution composed of approximately 5.5 mg ml^{-1} protein in 50 m*M* bis-tris pH 5.9, 20 m*M* ammonium sulfate, 7% PEG 3350, 25 m*M* 1,5-AF, 1 m*M* NADPH, which was equilibrated at 291 K as a hanging drop against reservoir solution consisting of 100 m*M* bis-tris pH 5.5, 50 m*M* ammonium sulfate, 20%(*w*/*v*) PEG 3350. Crystals belonging to the orthorhombic space group $C222_1$, with unit-cell parameters a = 68.9, b = 89.7, c = 94.5 Å, grew within 20 d. Prior to data collection, the crystals were soaked in a cryoprotection solution [100 m*M* bis-tris pH 5.5, 50 m*M* ammonium sulfate, 20%(*w*/*v*) PEG 3350, 28 m*M* 1,5-AF, 2 m*M* NADPH, 20%(*v*/*v*) PEG 400] and flash-cooled by rapid transfer into liquid nitrogen.

X-ray data were collected using a marμX system (MAR Research GmbH, Norderstedt, Germany) equipped with a mardtb desktop-beamline goniometer system, an IμS microfocus source (Incoatec, Geesthacht, Germany) for Cu $K\alpha$ radiation, a mar345 image-plate detector and a liquid-nitrogen Cryostream 700 (Oxford Cryosystems, Oxford, England).

The collected diffraction data were indexed, integrated and scaled using *XDS* (Kabsch, 1993, 2010*a*,*b*). The phases were obtained by molecular replacement using *MOLREP* (Vagin & Teplyakov, 2010). Using the crystal structure of AFR from *S. morelense* (PDB entry

2glx; Dambe *et al.*, 2006) as a template, a homology model with the correct amino-acid annotation was automatically generated using the *SWISS-MODEL* server (Schwede *et al.*, 2003). The search model for molecular replacement did not contain water molecules or bound cofactor. Several cycles of refinement with *REFMAC*5 (Murshudov *et al.*, 2011) as implemented in the *CCP*4 program suite (Winn *et al.*, 2011) and manual inspection and correction of the model with *Coot* (Emsley *et al.*, 2010) were performed to build the complete protein model with the NADP(H) cofactor. Structural representations were generated using *PyMOL* v.1.5 (DeLano, 2002).

3. Results and discussion

3.1. Structure determination

The bacterial AFR from *S. meliloti* 1021 was crystallized in complex with the cofactor NADP(H) in space group $C222_1$ with one molecule per asymmetric unit (V_M = 1.84 Å^3 Da^{-1}). Diffraction data were recorded to 1.93 Å resolution. For convenience, the crystal structure was determined by molecular replacement using a homology model derived from the structure of the homologous AFR from *S. morelense* as a search template (PDB entry 2glx; Dambe *et al.*, 2006). Refinement of the structure resulted in final crystallographic *R* factors of R_{work} = 15.4% and R_{free} = 20.7% with good geometry according to the Ramachandran plot (Laskowski *et al.*, 1993). The final model includes amino-acid residues 1–333, one NADP(H) cofactor and 291 water molecules. The protein structure was refined with individual temperature factors (*B* factors), resulting in an average crystallographic temperature factor over all atoms of 23.5 Å^2 (Table 1).

3.2. Overall structure

AFR from *S. meliloti* shares a sequence identity of 86% with AFR from *S. morelense* and features the same three-dimensional fold (Figs. 2 and 3). The enzyme is composed of two structural domains: an N-terminal domain and a larger C-terminal domain. The NADP(H) cofactor-binding site is located between the two domains (Fig. 3*b*). The domain formed by the first 120 amino-acid residues displays the typical dinucleotide-binding motif referred to as the Rossmann fold (Rossmann *et al.*, 1974), consisting of a central β-sheet composed of two β–α–β–α–β motifs. The cofactor NADP(H) is bound in a deep cleft above this β-sheet. The larger C-terminal domain (amino-acid residues 121–333) also possesses α/β topology and exhibits structural homology to members of the family of glyceraldehyde-3-phosphate dehydrogenase-like proteins. Biochemical characterization of the AFR from *S. morelense* revealed a monomeric enzyme in solution (Kühn *et al.*, 2006). In contrast, biochemical characterization of the AFR from *S. meliloti* using multi-angle laser light-scattering (MALLS; data not shown), size-exclusion chromatography and

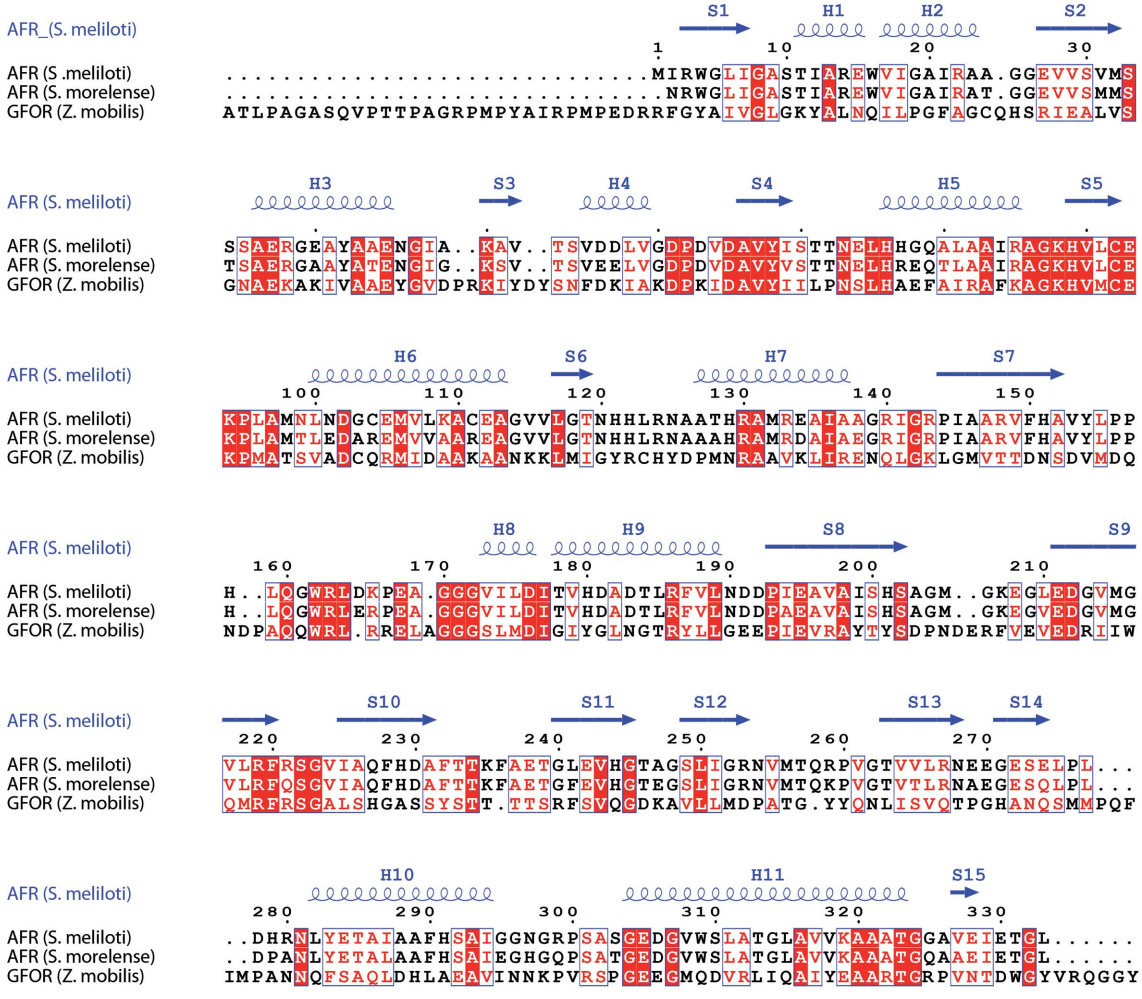

Figure 2
Sequence alignment of *S. meliloti* AFR with *S. morelense* AFR and with GFOR (Wiegert *et al.*, 1997). This figure was produced using *ESPript* (Gouet *et al.*, 2003).

MALDI mass spectrometry (Stosik, 2008) revealed a dimeric molecule in solution. In the crystal structure of *S. morelense* AFR, the asymmetric unit contains two enzyme molecules displaying a tight dimer. In the presented crystal structure of *S. meliloti* AFR, the asymmetric unit contains only one enzyme molecule; however, a tight dimer is generated with a symmetry mate. Interestingly, this dimer shows the same arrangement as the two enzyme molecules within the asymmetric unit of the *S. morelense* AFR structure. In order to evaluate the interfaces formed between the individual monomers within the crystal structure, we analyzed the intermolecular contacts formed by crystal packing using the *PISA* server at the European Bioinformatics Institute (*PDBePISA* v.1.46; Krissinel & Henrick, 2007). The analysis revealed one extended interface formed with the $(x, -y, -z)$ symmetry mate, covering an interface area of 1642 Å^2 with a solvation-energy gain $\Delta^{i}G$ of -66.1 kJ mol^{-1} and a complexation significance score (CSS) of 0.622, suggesting that the protein should exist as a dimer in solution. Interestingly, the interface analysis for AFR from *S. morelense* (PDB entry 2glx) revealed an even larger interface area of 1822 Å^2 but with a smaller solvation-energy gain $\Delta^{i}G$ of -60.3 kJ mol^{-1} and thus a lower complexation significance score of 0.452. For both proteins the dimer interface is formed between the large and extended β-sheet moiety of the C-terminal domain (Fig. 3*b*). Therefore, based on the individual crystal structures both enzymes might exist as dimers in solution, but this could only be verified biochemically for AFR from *S. meliloti* (Stosik, 2008).

3.3. The active site

We compared the crystal structure of *S. meliloti* AFR with the recently published structure of its closest relative, *S. morelense* AFR (PDB entry 2glx; Dambe *et al.*, 2006), and with the well characterized structure of glucose–fructose oxidoreductase (GFOR) from *Zymomonas mobilis* (PDB entry 1h6a; Nurizzo *et al.*, 2001; Wiegert *et al.*, 1997). The identity between *S. meliloti* AFR and *S. morelense* AFR is 86% (with an r.m.s.d. of 1.3 Å for 323 aligned residues out of 332 residues; *Z*-score of 50.6) and that between *S. meliloti* AFR and GFOR is 23% (with an r.m.s.d. of 2.4 Å for 324 aligned residues out of 381 residues; *Z*-score of 36.9). The comparison was performed by pairwise analysis using the *DALI* server (Hasegawa & Holm, 2009). The comparison with *S. morelense* AFR revealed only two large structural deviations within the protein fold. The two loop regions connecting β-strand S7 to α-helix H8 and connecting β-strand S8 to β-strand S9 (Fig. 4*a*) have an extended conformation in *S. meliloti* AFR and display higher flexibility and disorder (the average *B* factor for amino-acid residues 154–170 and 203–210 is around 75 Å^2). These two loop regions are not involved in crystal packing. They are positioned close to the putative active site and thus should influence the mode of substrate binding or product release. The conformations observed within the presented *S. meliloti* AFR structure can be interpreted as an open conformation, whereas the conformations observed in the structures of *S. morelense* AFR and GFOR display a closed conformation in respect to accessibility towards the substrate-binding site. Superimposing the crystal structures of the AFRs from *S. meliloti* and *S. morelense* reveals a concerted domain movement. Compared with *S. morelense* AFR, the two domains of *S. meliloti* AFR rotate approximately by 2° (N-terminal domain) and 2.5° (C-terminal domain), both to the outside (Fig. 4*a*). As a consequence, the binding cleft for the cofactor as well as for the substrate becomes more accessible. The electron density in the active site of *S. meliloti* AFR is poor for some parts of the cofactor NADP (high temperature factors, suggesting high flexibility) and although the crystals were grown in the presence of 25 m*M* 1,5-AF no electron density for the substrate was found. In contrast, acetate is bound within the active site of *S. morelense* AFR and succinate and glycerol are bound in that of GFOR. Thus, the conformation of *S. morelense* AFR and GFOR can be regarded as closed after induced-fit binding of the substrate and cofactor has occurred. In addition to the differences within the mentioned loop regions and the overall domain arrangement, the nicotinamide moiety displays a different orientation in comparison to the NADP(H) cofactor of 2glx and GFOR (Fig. 4*b*). The orientation observed in *S. meliloti* AFR cannot be adopted in *S. morelense* AFR and GFOR since the conserved residues Trp162–Arg163 (*S. morelense* AFR) and Trp251–Arg252 (GFOR) within the loop S7/H8 are positioned in too close a proximity to the nicotinamide when the loop is in its closed conformation. It seems to be likely that the nicotinamide moiety and the loop S7/H8 change their orientation in a concerted manner depending on the occupancy of the active site. Various strategies to obtain a structure of *S. meliloti* AFR with bound substrate, substrate analogue or competitive inhibitor failed. In order

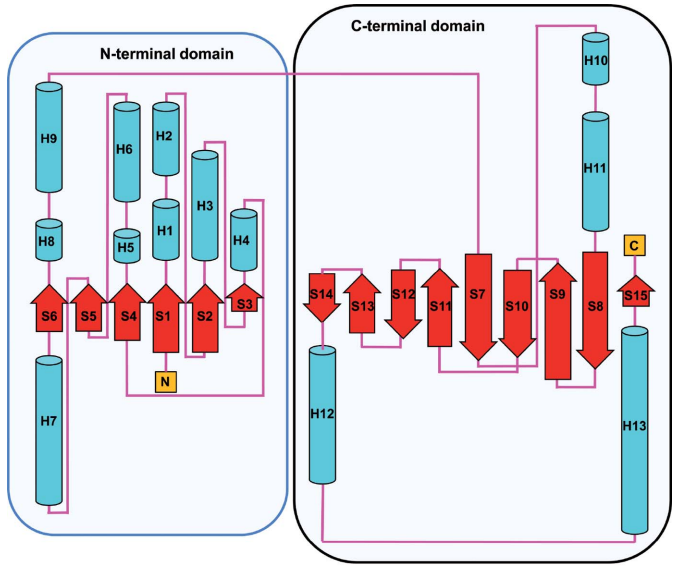

(*a*)

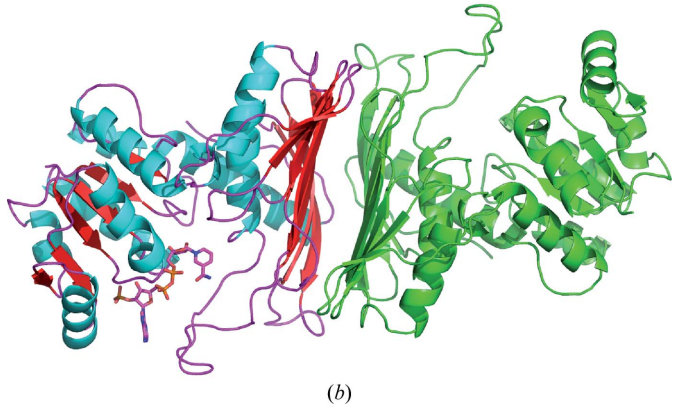

(*b*)

Figure 3
Topology of *S. meliloti* AFR. (*a*) Arrangement of the secondary-structure elements within one molecule. The figure was generated using *PDBsum* (Laskowski, 2009). (*b*) Ribbon representation of AFR and the putative dimeric assembly of the active enzyme. The secondary-structure elements of the molecule within the crystallographic asymmetric unit are coloured cyan (α-helices), red (β-sheets) and magenta (loops). The bound cofactor NADP(H) is displayed in ball-and-stick representation. The molecule in green represents the $(x, -y, -z)$ symmetry mate. Intermolecular contacts are formed between the two extended β-sheets of the C-terminal domain to build the stable dimer as observed in solution.

to obtain some insight into the molecular interactions for substrate binding, we performed docking simulations of the mode of binding of the substrate 1,5-AF and the product 1,5-AM within the active site using the program *AutoDock* v.4.2 (Morris *et al.*, 2009). The structure of *S. morelense* AFR was used to simulate the enzyme with a closed conformation of loop S7/H8 and its interaction with bound substrate and product, respectively (Figs. 4*c*, 4*d* and 4*e*). The docking simulations produced diverse conformations of bound substrate/product within the active site, with one dominant conformation. In the following we will interpret the two most likely orientations from these simulations and will put them into perspective for substrate binding and product release (Fig. 4*f*). In a comparison between 1,5-AF and 1,5-AM the orientations of the 3′-OH, 4′-OH and 6′-OH hydroxyl groups are in nearly the same positions; thus, their interactions with the side chains of amino-acid residues His151, Arg163 and Asp176 are maintained. The side chain of His151 can form two alternative hydrogen bonds *via* its NE2 atom: one to the 6′-OH and one to the endocyclic O atom of 1,5-AF. Owing to the reduction of the carbonyl

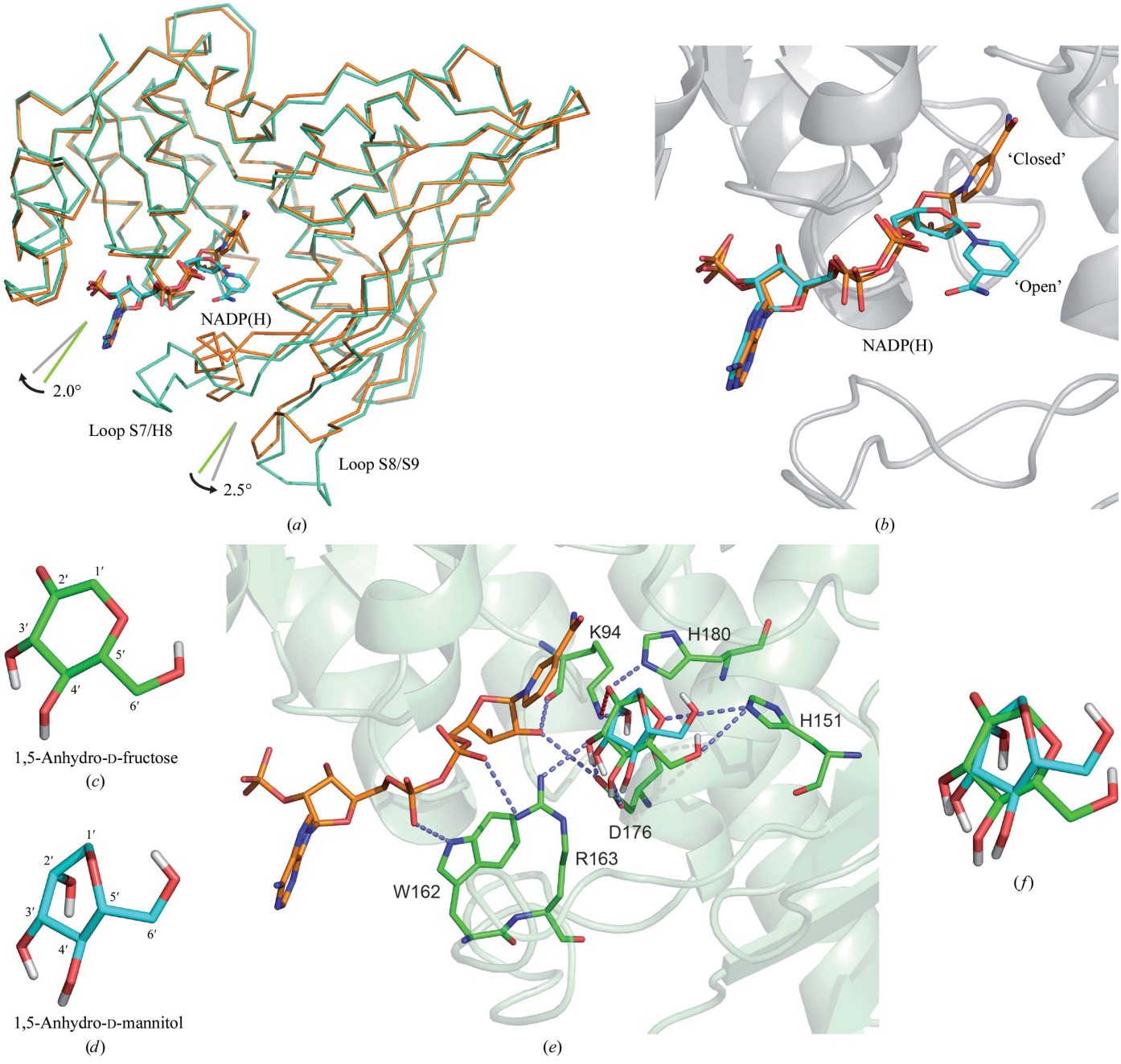

Figure 4
Open and closed conformations of AFR. (*a*) Superposition of the C^{α} main-chain trace of *S. meliloti* AFR (light green) and *S. morelense* AFR (orange). The cofactor NADP(H) is displayed in ball-and-stick representation (C atoms in cyan for *S. meliloti* and in orange for *S. morelense*, O atoms in red, N atoms in blue). The angle and arrows represent the relative movement of the N-terminal and C-terminal domains of *S. meliloti* AFR relative to *S. morelense* AFR. (*b*) Close-up view of the cofactor binding mode. (*c*–*f*) Representation of 1,5-AF (*c*) and 1,5-AM (*d*) in the conformation identified by docking simulations. (*e*) Active site of AFR (*S. morelense*) with docked substrate 1,5-AF and product 1,5-AM. The amino-acid residues interacting with the sugar molecules are highlighted in ball-and-stick representation, with potential hydrogen bonds shown as dotted lines. The figures were produced using *PyMOL* v.1.5 (DeLano, 2002).

group at the 2′ C atom, the O atom at the 2′ C atom and the endocyclic O atom adopt new positions. Since His151 remains in its orientation owing to the interaction with the 6′-OH hydroxyl group, formation of the hydrogen bond between the endocyclic O atom and His151 NE2 is no longer possible. Furthermore, His180 is released since the hydrogen bond formed between the carbonyl O atom of 1,5-AF and the side-chain atom His180 NE2 is lost. In addition, the reduced O atom (2′-carbonyl→2′-hydroxy) rearranges and therefore the interacting side chain of Lys94 adopts a new conformation. This rearrangement of Lys94 might serve as a molecular switch for triggering product release. Since Lys94 also interacts with the 2′-OH group of the nicotinamide ribose moiety, the structural reorientation of Lys94 might trigger a conformational rearrangement of the ribose sugar and thus rotational reorientation of the nicotinamide ring. As a consequence of the movement of the nicotinamide moiety towards amino-acid residues Trp162 and Arg163, these side chains have to move away, releasing their interaction with the pyrophosphate moiety of the NADP cofactor and thus inducing even more flexibility to the cofactor and less strain upon reorientation of the nicotinamide moiety. Arg163 forms a hydrogen bond to the 3′-OH group of the substrate and product. Upon reorientation of Arg163 this interaction is lost and release of the product is facilitated. The amino-acid side chain of Asp176 is observed in two alternative conformations. While one conformation forms a hydrogen bond to the 3′-OH and 4′-OH groups, the other does not. Owing to the rearrangement within the region Trp162–Arg163 the second conformation is favoured, allowing the product to be pulled out from the active site, thus further reducing interaction with the product and favouring its release from the enzyme. In a final step loop S7/H8 completely rearranges and the product is released.

In conclusion, we propose that the observed orientations of the presented residues of *S. meliloti* AFR represent a conformation after the release of the product, whereas the structure of *S. morelense* AFR represents a structure shortly before or after reduction with bound substrate or product. The outlined stepwise rearrangement within the active site and the adjacent loop is most likely to be triggered by the reorientation of the side chain of Lys94, thus giving it the role of a molecular switch. A similar role was proposed for the corresponding Lys181 in GFOR, where the different observed conformations favour or discriminate the binding of substrate or product (Nurizzo *et al.*, 2001).

We gratefully acknowledge access to the core facilities of the ZBM/LMB of the CAU. Additionally, we are grateful for access to the HTX crystallization facility at the EMBL Outstation (Hamburg, Germany). We would like to thank Drs Yvonne Carius, Tresfore Dambe and Ulrich Zander for helpful discussions. This work was supported by the Deutsche Bundesstiftung Umwelt (Az 13195-32) within the research network ChemBioTec.

References

Ahrén, B., Holst, J. J. & Yu, S. (2000). *Eur. J. Pharmacol.* **397**, 219–225.
Ahrén, B. & Yu, S. (2002). US Patent WO 2001051058 A1.
Andersen, S. M., Lundt, I., Marcussen, J. & Yu, S. (2002*a*). *Carbohydr. Res.* **337**, 873–890.
Andersen, S. M., Lundt, I., Marcussen, J. & Yu, S. (2002*b*). US Patent WO 2000056745 A1.
Brünger, A. T. (1992). *Nature (London)*, **355**, 472–475.
Capela, D. *et al.* (2001). *Proc. Natl Acad. Sci. USA*, **98**, 9877–9882.
Cruickshank, D. W. J. (1999). *Acta Cryst.* D**55**, 583–601.
Dambe, T. R., Kühn, A. M., Brossette, T., Giffhorn, F. & Scheidig, A. J. (2006). *Biochemistry*, **45**, 10030–10042.
Delano, W. L. (2002). *PyMOL*. http://www.pymol.org.
Diederichs, K. & Karplus, P. A. (1997). *Nature Struct. Biol.* **4**, 269–275.
Dworacka, M. & Winiarska, H. (2005). *Dis. Markers*, **21**, 127–132.
Emsley, P., Lohkamp, B., Scott, W. G. & Cowtan, K. (2010). *Acta Cryst.* D**66**, 486–501.
Engh, R. A. & Huber, R. (1991). *Acta Cryst.* A**47**, 392–400.
Fiskesund, R., Abeyama, K., Yoshinaga, K., Abe, J., Yuan, Y. & Yu, S. (2010). *Planta Med.* **76**, 1635–1641.
Fujisue, M., Muroya, K., Nozaki, K., Yajima, M. & Yoshinaga, K. (2003). US Patent WO 2001056408 A1.
Gouet, P., Robert, X. & Courcelle, E. (2003). *Nucleic Acids Res.* **31**, 3320–3323.
Hasegawa, H. & Holm, L. (2009). *Curr. Opin. Struct. Biol.* **19**, 341–348.
Hirano, K., Ziak, M., Kamoshita, K., Sukenaga, Y., Kametani, S., Shiga, Y., Roth, J. & Akanuma, H. (2000). *Glycobiology*, **10**, 1283–1289.
Kabsch, W. (1993). *J. Appl. Cryst.* **26**, 795–800.
Kabsch, W. (2010*a*). *Acta Cryst.* D**66**, 133–144.
Kabsch, W. (2010*b*). *Acta Cryst.* D**66**, 125–132.
Kametani, S., Shiga, Y. & Akanuma, H. (1996). *Eur. J. Biochem.* **242**, 832–838.
Kim, M. J., Jung, H. S., Hwang-Bo, Y., Cho, S. W., Jang, H. C., Kim, S. Y. & Park, K. S. (2011). *Acta Diabetol.*, doi:10.1007/s00592-011-0302-0.
Kingston, R. L., Scopes, R. K. & Baker, E. N. (1996). *Structure*, **4**, 1413–1428.
Konishi, Y., Hashima, K. & Kishida, K. (2000). *Biosci. Biotechnol. Biochem.* **64**, 2462–2465.
Krissinel, E. & Henrick, K. (2007). *J. Mol. Biol.* **372**, 774–797.
Kühn, A., Yu, S. & Giffhorn, F. (2006). *Appl. Environ. Microbiol.* **72**, 1248–1257.
Laskowski, R. A. (2009). *Nucleic Acids Res.* **37**, D355–D359.
Laskowski, R. A., MacArthur, M. W., Moss, D. S. & Thornton, J. M. (1993). *J. Appl. Cryst.* **26**, 283–291.
Lee, S. S., Yu, S. & Withers, S. G. (2003). *Biochemistry*, **42**, 13081–13090.
Lichtenthaler, F., El Ashry, E. & Göckel, V. (1980). *Tetrahedron Lett.* **21**, 1429–1432.
Lundt, I. & Yu, S. (2010). *Carbohydr. Res.* **345**, 181–190.
Morris, G. M., Huey, R., Lindstrom, W., Sanner, M. F., Belew, R. K., Goodsell, D. S. & Olson, A. J. (2009). *J. Comput. Chem.* **30**, 2785–2791.
Murshudov, G. N., Skubák, P., Lebedev, A. A., Pannu, N. S., Steiner, R. A., Nicholls, R. A., Winn, M. D., Long, F. & Vagin, A. A. (2011). *Acta Cryst.* D**67**, 355–367.
Nurizzo, D., Halbig, D., Sprenger, G. A. & Baker, E. N. (2001). *Biochemistry*, **40**, 13857–13867.
Rossmann, M. G., Moras, D. & Olsen, K. W. (1974). *Nature (London)*, **250**, 194–199.
Sakuma, M., Kametani, S. & Akanuma, H. (1998). *J. Biochem.* **123**, 189–193.
Schwede, T., Kopp, J., Guex, N. & Peitsch, M. C. (2003). *Nucleic Acids Res.* **31**, 3381–3385.
Shiga, Y., Kametani, S., Kadokura, T. & Akanuma, H. (1999). *J. Biochem.* **125**, 166–172.
Stosik, B. (2008). PhD thesis. Saarland University, Germany.
Susumu, H., Junichi, A., Toshiyasu, M., Kazuhiro, Y., Hideto, I. & Masamitsu, F. (2002). Japan Patent 2002-027945.
Susumu, H., Yasuhito, T., Junichi, A., Kenkou, M., Kazuhiro, Y., Mami, F. & Hideto, I. (2003). US Patent WO 2001072124 A1.
Tickle, I. J., Laskowski, R. A. & Moss, D. S. (2000). *Acta Cryst.* D**56**, 442–450.
Vagin, A. & Teplyakov, A. (2010). *Acta Cryst.* D**66**, 22–25.
Vaguine, A. A., Richelle, J. & Wodak, S. J. (1999). *Acta Cryst.* D**55**, 191–205.
Weiss, M. S. (2001). *J. Appl. Cryst.* **34**, 130–135.
Wiegert, T., Sahm, H. & Sprenger, G. A. (1997). *J. Biol. Chem.* **272**, 13126–13133.
Winn, M. D. *et al.* (2011). *Acta Cryst.* D**67**, 235–242.
Yamanouchi, T., Inoue, T., Ichiyanagi, K., Sakai, T. & Ogata, N. (2003). *Biochim. Biophys. Acta*, **1623**, 82–87.
Yu, S. (2008). *IUBMB Life*, **60**, 798–809.
Yu, S. & Fiskesund, R. (2006). *Biochim. Biophys. Acta*, **1760**, 1314–1322.
Yu, S., Kenne, L. & Pedersén, M. (1993). *Biochim. Biophys. Acta*, **1156**, 313–320.
Yu, S. & Pedersén, M. (1993). *Planta*, **191**, 137–142.
Yu, S., Refdahl, C. & Lundt, I. (2004). *Biochim. Biophys. Acta*, **1672**, 120–129.
Zachariou, M. & Scopes, R. K. (1986). *J. Bacteriol.* **167**, 863–869.